PHYSICS

Orbital angular momentum multiplication in plasmonic vortex cavities

Grisha Spektor[1,2,3]*, Eva Prinz[4], Michael Hartelt[4], Anna-Katharina Mahro[4], Martin Aeschlimann[4], Meir Orenstein[1]

Orbital angular momentum of light is a core feature in photonics. Its confinement to surfaces using plasmonics has unlocked many phenomena and potential applications. Here, we introduce the reflection from structural boundaries as a new degree of freedom to generate and control plasmonic orbital angular momentum. We experimentally demonstrate plasmonic vortex cavities, generating a succession of vortex pulses with increasing topological charge as a function of time. We track the spatiotemporal dynamics of these angularly decelerating plasmon pulse train within the cavities for over 300 femtoseconds using time-resolved photoemission electron microscopy, showing that the angular momentum grows by multiples of the chiral order of the cavity. The introduction of this degree of freedom to tame orbital angular momentum delivered by plasmonic vortices could miniaturize pump probe–like quantum initialization schemes, increase the torque exerted by plasmonic tweezers, and potentially achieve vortex lattice cavities with dynamically evolving topology.

INTRODUCTION

Orbital angular momentum (OAM) of light has been of wide interest in recent years (*1*–*6*), laying the foundation for promising applications such as reshaping light-matter interactions (*7*, *8*), optical tweezing (*9*–*12*), optical communications (*13*–*15*), and quantum information processing (*16*). The confinement of OAM to a surface enabled access and control to new physical phenomena (*17*, *18*) including linear spin-orbit conversion (*19*–*21*), orbit-orbit conversion (*22*), and nonlinear spin-orbit mixing (*23*). Recent experimental access to the subcycle surface plasmon polariton (SPP) dynamics (*24*–*26*) enabled the study of the dynamical evolution of a vortex (*27*) and direct determination of its angular momentum, as well as revealed the dynamics of plasmonic nanofocusing (*28*, *29*), thus raising the possibility of temporal OAM control. In parallel, the ability to generate vortex lattices (*30*–*33*) and the emergence of their topological properties (*34*, *35*) are of great current interest to the scientific community (*36*, *37*). Revealing and taming new degrees of freedom for generating and controlling OAM are thus key to the advancement of the field.

The generation and shaping of plasmonic fields are typically achieved by engraving boundaries in a metal and exciting them with a certain illumination (*20*, *21*, *24*, *25*, *28*, *29*, *34*, *35*, *37*–*45*). Be it continuous engravings or local geometries forming meta-slits (*43*, *46*–*50*), it is generally widely assumed that the generated fields are set by the initial interaction with the static boundaries of the engraved structures. Even more so, in the case of plasmonic OAM generation and control, it has practically become a paradigm that the boundaries defined by a conventional plasmonic vortex generator create a single vortex, well described by a single Bessel distribution (*19*–*21*, *27*, *28*, *44*). This is not to be confused with more elaborate excitation structures that allow for the generation of compound fields (*51*, *52*).

In this work, we challenge this paradigm. We experimentally demonstrate that after the initial SPP vortex is excited by the boundaries, it subsequently interacts with the boundaries, resulting in partial reflections. We show that these reflections form successive, previously unobserved higher-order vortices, gaining additional angular momentum at each reflection (Fig. 1, A to C). We demonstrate that even a slit geometry has weak-yet-measurable contributions to these high-order vortices. To increase the reflected power, we construct a plasmonic vortex cavity with ultraflat gold surfaces and golden wall mirrors created by template stripping (*53*–*57*). Using this cavity (Fig. 1, D to F), we produce a train of plasmonic vortices with dynamically increasing large OAM and decelerating angular velocity (see movies S1 to S3). Using a time-resolved normal-incidence pump-probe scheme (Fig. 1F) in time-resolved photoemission electron microscopy (TR-PEEM) (*26*), we resolve the complex dynamics within the decelerating cavities, separating the successive vortex pulses in time and space and quantifying the rules governing the OAM growth. The flatness of our surface provides low scattering losses, allowing us to record dynamics for the long duration of about 330 fs corresponding to ~100 μm of accumulated propagation inside the cavity.

RESULTS

The formation of a plasmonic vortex is achieved when an azimuthally varying boundary in the form of an Archimedean spiral, $r(\theta) = r_i + \lambda_{spp} \cdot m\theta/2\pi$, is illuminated with properly polarized light (*19*, *21*). Here, r is the distance of the boundary from the center, r_i is the minimal distance, λ_{spp} is the plasmonic wavelength, m is the chiral order of the spiral structure, and θ is the azimuthal coordinate. To excite high-order vortices with an Archimedean spiral, a large m is required. This causes significant propagation distance differences between plasmons originating from different locations along the slit, resulting in angularly dependent losses that distort the vortex. To mitigate this, the spiral is segmented to the form $r_m(\theta) = r_i + \lambda_{spp} \cdot \mathrm{mod}(m\theta, 2\pi)/2\pi$, resulting in a maximal path difference of λ_{spp} within each segment while still providing the necessary phase, allowing the formation of high-order vortices. In a typical setting, a spiral structure of order m is illuminated by circularly

[1]Department of Electrical Engineering, Technion - Israel Institute of Technology, 32000 Haifa, Israel. [2]Time and Frequency Division, Associate of the National Institute of Standards and Technology, Boulder, CO 80305, USA. [3]Department of Physics, University of Colorado, Boulder, CO 80309, USA. [4]Department of Physics and Research Center OPTIMAS, University of Kaiserslautern, Erwin Schroedinger Strasse 46, 67663 Kaiserslautern, Germany.
*Corresponding author. Email: grisha.spektor@gmail.com

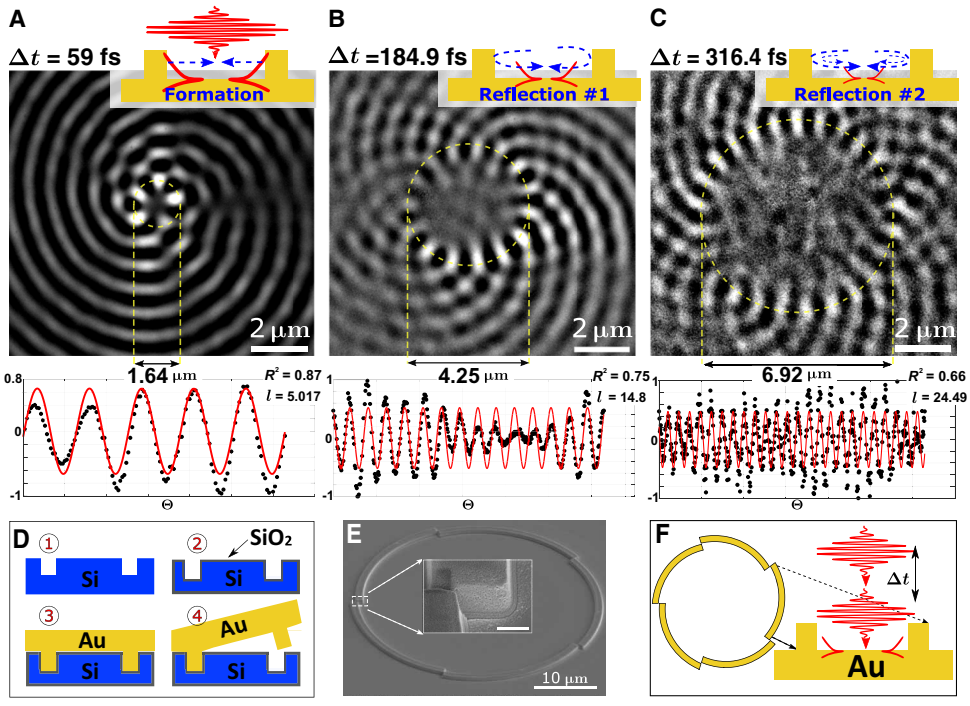

Fig. 1. Concept of plasmonic vortex cavities. Experimental results (**A** to **C**) within a plasmonic vortex cavity of order $m = 5$, showing the revolution stages (*27*) of the initial vortex of order $l = 5 + 1$ (A) and subsequent first (B) and second (C) reflections of the wave packet, forming vortices of orders $l = 15 + 1$ and $l = 25 + 1$, respectively. The snapshots show 5, 15, and 25 azimuthal lobes imprinted into the photoemitted electrons due to the nonlinear mechanism of our technique (*23*). The bottom insets show azimuthal and radial fitting of the diameter and the number of lobes in the main vortex signal. (**D**) Schematic of the template stripping process used to fabricate plasmonic vortex cavities with ridge mirrors; ① focused ion beam milling of the inverse cavity in silicon, ② thermal oxide growth, ③ Au sputtering, and ④ stripping. (**E**) Scanning electron microscopy image of a template stripped vortex cavity of order $m = 5$. Scale bar (inset), 500 nm. (**F**) Pump-probe setup schematic showing two ~23-fs pulses with a center wavelength of 800 nm (red) impinging on the sample at normal incidence with interferometrically controlled time delay Δt used in the TR-PEEM setup.

polarized light with $\sigma = \pm 1$. One can describe an SPP pulse forming the vortex in the time domain by extending the schematic representation established by (Fig. 2) (*43*). The excitation of SPPs takes place at the boundaries while imprinting an azimuthal phase delay, which can be envisioned on an imaginary line equidistant from the center (Fig. 2A). Then, the still inward-propagating SPPs interfere with the already-outward propagating SPPs, forming the revolution stage of the vortex (Fig. 2B). Subsequently, the vortex dissolves when the wave packet becomes predominantly outward-propagating, leaving the center of the structure while maintaining its azimuthal phase (Fig. 2C). The experiments reported to date show great agreement with this description. It is accepted that in a sufficiently large structure, the electric field components at the vortex revolution stage/phase are very well approximated by a Bessel functional form given by, $E_z \approx J_l(k_{spp}r) \times \exp(il\theta)$, $E_r \approx J_l'(k_{spp}r) \times \exp(il\theta)$, and $E_\theta \approx J_l(k_{spp}r) \times \exp(il\theta)$ (see the Supplementary Materials), where J_l is the Bessel function of order l; J_l' is its first derivative; r, θ, and z are the cylindrical coordinates; k_{spp} is the plasmonic wave number; and $i = \sqrt{-1}$. The vortex is then said to be of order l and in the case of circularly polarized illumination $l = m + \sigma$. Historically, the out-of-plane field component is the one mainly discussed in the literature due to its accessibility using scanning near-field optical microscopy techniques. For continuity, we follow this practice here as well. It should be noted that our time-resolved normal-incidence PEEM measurements are only sensitive to the in-plane field components of the SPPs, except for a static contribution from the out-of-plane plasmon field (a more detailed description is given in the Supplementary Materials). Except for its amplitude, the E_θ field is identical to E_z, and E_r has a different vortex radius but the same number of lobes.

When the outward-propagating SPPs meet the boundaries that launched them, they are partially back-reflected and go back toward the center of the structure (Fig. 2D). Notably, at each azimuthal location, the SPPs traverse the region enclosed between the imaginary dashed circular line and the physical boundaries of the structure twice, once before the reflection and once after. The reflected SPPs thus obtain an additional azimuthal phase equal to twice the order of the structure that results in the formation of a new vortex of the form

$$E_z \approx J_{l+2\cdot m}(k_{spp}r) \cdot e^{-i(l+2m)\theta} \quad (1)$$

This reflected vortex has different radial and azimuthal spatial distributions compared to the initial vortex, and in a steady-state measurement, their fields are overlaid. The azimuthal wave number of this reflected vortex, or its topological charge, is given by $k_\theta = l + 2m$ and is increased by twice the order of the structure, while its angular velocity $\omega_\theta = 2\pi/k_\theta$ is respectively decelerated.

So far, neither such a reflected vortex nor any other subsequent vortices have been experimentally observed. As we show in Fig. 3 (A and B), the predominantly explored slit geometry has poor reflectance (Fig. 3B) of up to a maximum of 16%. Moreover, the slit

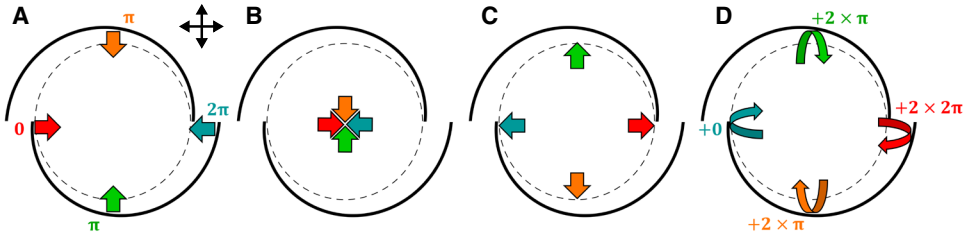

Fig. 2. Schematic description of a round trip within a plasmonic vortex cavity. (**A**) A vortex generator of order $m = 2$ illuminated by radially polarized light (solid black arrows) generates counterpropagating SPPs with azimuthally varying phase delay (colored arrows) as depicted at the imaginary dashed circle concentric with the generator. (**B**) The plasmonic vortex is generated when the inward-propagating SPP wave packets combine at the center and form a phase singularity. (**C**) After passing through the center, the outgoing wave packets keep the relative phase differences until they reach the imaginary dashed circle. (**D**) The SPPs propagate up to the cavity boundaries where they are partially reflected and propagate inward toward the center again, thus accumulating azimuthally varying relative phases corresponding to twice the geometric phase of the cavity [following the schematic representation established by (*43*)].

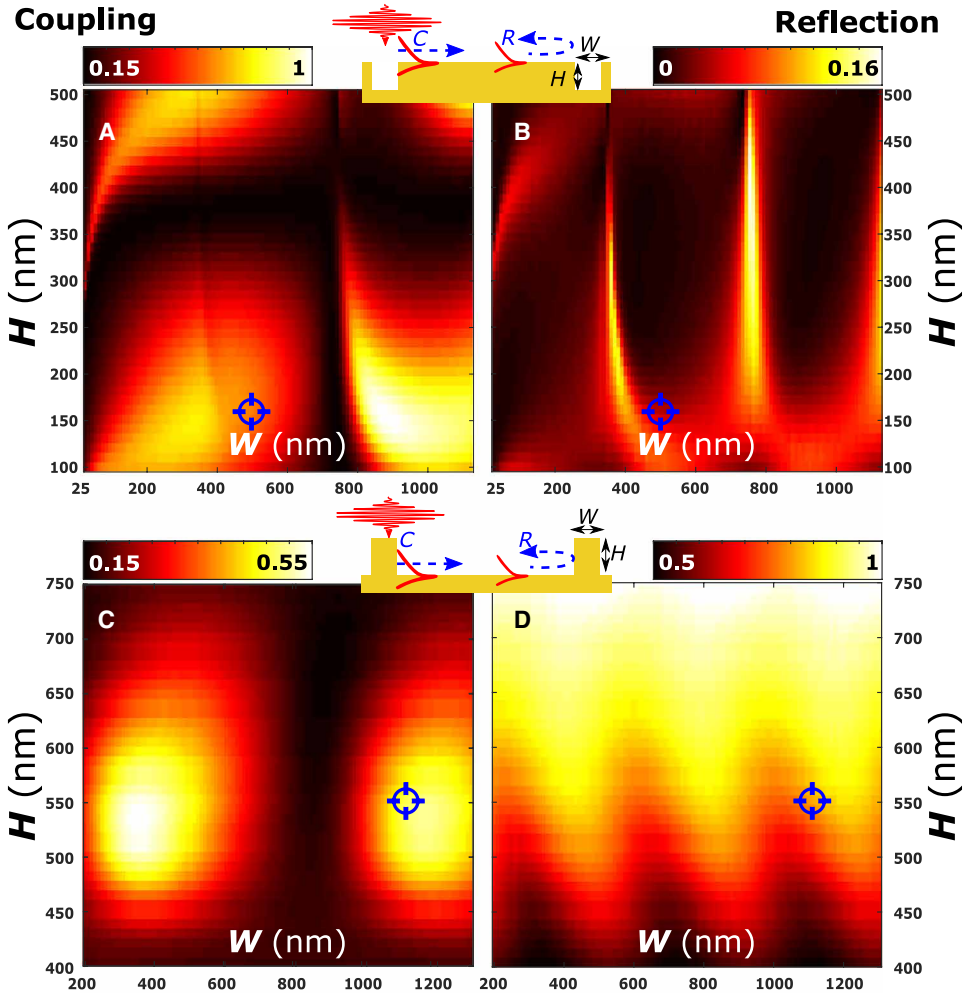

Fig. 3. Efficiency Simulations. Finite-difference time-domain calculations of coupling efficiency (**A** and **C**) and reflection (**B** and **D**) of a slit/ridge as a function of height and width. It can be seen that a ridge structure can function simultaneously as an efficient coupler and nearly perfect reflector, whereas the slit cannot. The blue crosshairs show our fabricated slit structure having $W = 500$ nm and $H = 160$ nm, while the ridge structure has $W = 1110$ nm and $H = 550$ nm, resulting in ~85% reflection at nearly maximal coupling strength accessible by the fabrication method.

reflectance maxima are not aligned with the coupling efficiency maxima in the structural parameter space, and therefore, slits do not perform as simultaneously good couplers and reflectors. Last, in addition to the poor reflectance, plasmonic propagation losses further diminish the SPP power in the reflected plasmons by the time they reach the center to the formation of reflected vortices. The last two reasons and the lack of time resolution in previous experimental work practically eliminated the reflections from the experiments

and solidified the notion of obtaining a single vortex from spiral-shaped vortex generators within the community.

In the following, we experimentally demonstrate that using the time-resolved signal obtained by TR-PEEM and a proper slit or ridge design, the generation of higher-order vortices (Fig. 4) by reflection can be enhanced and made detectable. For our study, we use a 160-nm gold layer sputtered onto a silicon substrate and mill 500-nm-wide slits using a focused ion beam, forming a plasmonic vortex generator of order $m = 5$. The measurement was performed by TR-PEEM. To detect the weak slit-reflected vortex, we used the time-delay Fourier filtering technique of the TR-PEEM signal that increases the signal-to-noise ratio of the desired contribution. In this process, the raw PEEM data are pixel wise–filtered in the time delay–conjugated domain to contain only the dynamic contributions that oscillate with ω, where $\omega = 2\pi c/\lambda_0$ is the frequency of light at $\lambda_0 = 800$ nm (see the Supplementary Materials for details) (*23*).

Figure 4 shows snapshots of the propagating vortex taken with the probe pulse at a time delay Δt after the launching of the vortex by the pump pulse at the boundaries. Note that because of the nonlinear subtractive spin-orbit coupling between the circularly polarized light of the probe pulse and the propagating plasmonic vortex, inherent to the TR-PEEM imaging process (*23*), the number of lobes in the experimentally resolved image differs from the propagating plasmonic vortex (l) by $-\sigma$ ($l_{exp} = l - \sigma$), which means that the helicity of the probe pulse has to be subtracted. Figure 4A shows the first vortex of order 6 measured with right-handed circularly polarized light ($\sigma = 1$) resulting in $l_{exp} = 6 - 1 = 5$ azimuthal lobes. The snapshot is taken 58.5 fs after the launching of the plasmonic pulse by the boundaries. Figure 4B is taken 79 fs later, 137.5 fs after the launching of the pulse. It shows 15 azimuthal lobes corresponding to a plasmonic vortex of order $l = 16$. During 137.5 fs, the plasmons propagate $d_{prop} \sim 41.25$ μm, and in a vortex generator with a radius of 12 μm, this corresponds to slightly more than one and a half round trips within the structure. We thus observe a fully developed vortex of order $l = 16$ within the plasmonic vortex generator of order $l = 5$, corresponding to a vortex that is created because of the reflections of the plasmons from the slits defining the structure.

The propagation loss associated with the distance traveled by the plasmons is given by $l_{prop} = \exp(-\Im(k_{spp}) \cdot d_{prop})$, where $\Im(k_{spp})$ is the imaginary part of the plasmonic wave number. The reflectance of the slit with our parameters shown in Fig. 3B is $r_{slit} = 0.1$. The slit-reflected vortex is, therefore, $l_{prop} \times (1 - r_{slit})$ times weaker than the original vortex, to the extent that it is not visible in the raw TR-PEEM signal.

To truly use and control the reflection-generated high-order vortices, one must increase their relative intensity. We achieve that by augmenting the conventional plasmonic vortex generator and forming a plasmonic vortex cavity with boundaries consisting of golden walls (ridge structure) instead of slits. As shown in Fig. 3 (C and D), although golden ridges couple 45% less energy from the impinging light pulse into the plasmons than slits do, they can achieve almost perfect reflectance. As opposed to slits, golden ridges can serve both as good couplers and nearly perfect reflectors as the two efficiency maxima are aligned. Our ridge design facilitates ~85% reflectivity for a wide range of incidence angles, enabling the vortex generation within the cavity. This contrasts with Bragg gratings that while achieving similar reflectivity and improved coupling using many grating periods (*58*), do so only for a narrow range of incident plasmonic wave vector angles and wavelengths.

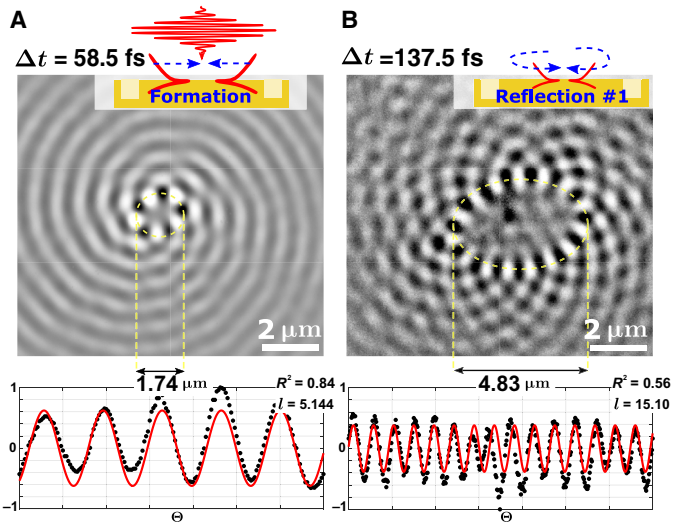

Fig. 4. Experimental result of a cavity of order $m = 5$ made with a slit reflector. (**A**) Formation stage of the initial vortex of order $l = 5 + 1$ and the subsequent first (**B**) reflection of the wave packet, forming a vortex of order $l = 15 + 1$. The snapshots show 5 and 15 azimuthal lobes imprinted into the photoemitted electrons due to the nonlinear mechanism of our technique (*23*). The bottom insets show azimuthal and radial fitting of the diameter and the number of lobes in the main vortex signal. The vortices are elliptically deformed because of a slight tilt misalignment of the ion beam stage during the sample fabrication (see fig. S10).

The results in Fig. 1 (A to C) show a cavity of order 5, which is excited with right-hand circularly polarized light ($\sigma = 1$), resulting in a vortex of order 6 (Fig. 1A) and two subsequent vortices of orders $l = 16$ and $l = 26$ upon two consecutive reflections. The vortices show 5, 15, and 25 azimuthal lobes due to the nonlinear interaction with the probe pulse as discussed above, and the radial distributions correspond well to the theory (see the Supplementary Materials). The first and second reflections are imaged at subsequent time delays of 125.9 and 131.5 fs and correspond to ~37.77 and ~ 39.45 μm traveled by the plasmons, respectively. This distance is within the pulse duration correspondence to a round trip (from the center and back) within the cavity having $r_i = 18$ μm. The limiting factor for observing the higher-order reflections is the maximal physical retardation of our delay stage.

We thus obtain theoretically and experimentally that, for a continuous-wave experiment, the steady-state field distribution within plasmonic vortex generators and vortex cavities, in particular, is actually given by

$$E \approx \sum_n a_n \cdot J_{l+2\cdot n\cdot m}(k_{spp} r) \cdot e^{-i(l+2nm)\theta} \quad (2)$$

where a_n is a proportionality coefficient convoluting the reflection coefficient and the losses accumulated by propagation within the cavity between each subsequent reflection. This is in contrast to the widely assumed single term $J_l(k_{spp} r) \cdot e^{-il\theta}$. Our finding shows that the nth generated vortex pulse carries OAM of the order $l_n = l + 2{\cdot}n{\cdot}m$, indicating that each subsequent interaction with the boundaries of a vortex cavity of order m decelerates the angular velocity by providing additional $2{\cdot}m$ units of OAM.

DISCUSSION

From a physics standpoint, we have here an interesting cavity that has chiral mirrors that are nonlocal with respect to angular momentum. While regular mirrors of a cavity are local, reflecting the impinging field uniformly, reflection from a photonic crystal or a transverse grating is nonlocal (*59*), transferring linear momentum to the reflected fields. Here, we have a chiral mirror that is nonlocal with regard to angular momentum. The chirality breaks the symmetry so that any reflection always increases the angular momentum. This contrasts with reflection from typical gratings, which are nonlocal with respect to linear momentum and provide both an increase and decrease in the linear momentum by the reciprocal vector of the grating.

Our results provide an experimental glance into a decelerating cavity, revealing how the boundary conditions of the cavity produce temporally increasing topological charge producing higher OAM modes with each reflection. By quantifying the rule governing the progression of the OAM pulse train within these cavities, we thus introduce a new degree of freedom—the reflection from structural boundaries—as a tool to tame surface-confined OAM. Besides the fundamental interest posed by nonlocal cavities and going beyond the paradigms established in the plasmonic community, we believe that plasmonic vortex cavities could be used to miniaturize time-windowing techniques such as pump probe–like quantum initialization schemes, and the torque exerted by the vortex train may be used to increase the rotational power of plasmonic tweezers and enable the study of new phenomena as the breakdown of plasmonic vortices when the reflection-generated vortices become larger than the cavity. By combining the presented cavities with a spatially distributed gain medium, they could potentially be used as tunable generators of high-order OAM. Last, future studies of vortex lattice cavities could reveal how the cavity is populated with lattices having a temporally evolving topology.

MATERIALS AND METHODS

To construct a ridge-based plasmonic cavity, we used the process of template stripping (Fig. 1D) (*53*, *55*–*57*). We began with patterning a single crystalline silicon substrate with the negative image of the desired cavity. After native oxide removal, we grew a 50-nm-thick thermal oxide layer and sputtered a 700-nm layer of gold without any adhesion layer. In the final stage, the top surface of the gold was glued onto a glass substrate and peeled off the silicon template (see full recipe in the Supplementary Materials). The resulting structure provides a flat golden surface and the desired ridges (Fig. 1E). A summary of all structure parameters can be found in the Supplementary Materials.

All time-resolved two-photon photoemission experiments were performed at a normal-incidence photoemission electron microscope from Focus GmbH at the University of Kaiserslautern, providing up to 40-nm spatial resolution. A Ti:sapphire oscillator (Tsunami from Newport Spectra Physics) was used to create ultrashort (<30 fs) laser pulses at a central wavelength of 800 nm with a repetition rate of 75 MHz. In the pump-probe experiments, each laser pulse was split into two pulses, which were time-delayed with respect to each other in an actively phase-stabilized Mach-Zehnder interferometer (*60*) that provides temporal stability of less than 100 as. Time traces of the full experiment are available in the Supplementary Materials.

SUPPLEMENTARY MATERIALS

Supplementary material for this article is available at http://advances.sciencemag.org/cgi/content/full/7/33/eabg5571/DC1

REFERENCES AND NOTES

1. L. Allen, M. W. Beijersbergen, R. J. C. Spreeuw, J. P. Woerdman, Orbital angular momentum of light and the transformation of Laguerre-Gaussian laser modes. *Phys. Rev. A* **45**, 8185–8189 (1992).
2. A. M. Yao, M. J. Padgett, Orbital angular momentum: Origins, behavior and applications. *Adv. Opt. Photonics* **3**, 161–204 (2011).
3. K. Y. Bliokh, F. Nori, Transverse and longitudinal angular momenta of light. *Phys. Rep.* **592**, 1–38 (2015).
4. H. Rubinsztein-Dunlop, A. Forbes, M. V. Berry, M. R. Dennis, D. L. Andrews, M. Mansuripur, C. Denz, C. Alpmann, P. Banzer, T. Bauer, E. Karimi, L. Marrucci, M. Padgett, M. Ritsch-Marte, N. M. Litchinitser, N. P. Bigelow, C. Rosales-Guzmán, A. Belmonte, J. P. Torres, T. W. Neely, M. Baker, R. Gordon, A. B. Stilgoe, J. Romero, A. G. White, R. Fickler, A. E. Willner, G. Xie, B. McMorran, A. M. Weiner, Roadmap on structured light. *J. Opt.* **19**, 013001 (2017).
5. S. Franke-Arnold, N. Radwell, Light served with a twist. *Opt. Photon. News* **28**, 28–35 (2017).
6. Y. Shen, X. Wang, Z. Xie, C. Min, X. Fu, Q. Liu, M. Gong, X. Yuan, Optical vortices 30 years on: OAM manipulation from topological charge to multiple singularities. *Light Sci. Appl.* **8**, 90 (2019).
7. N. Rivera, I. Kaminer, B. Zhen, J. D. Joannopoulos, M. Soljačić, Shrinking light to allow forbidden transitions on the atomic scale. *Science* **353**, 263–269 (2016).
8. C. T. Schmiegelow, J. Schulz, H. Kaufmann, T. Ruster, U. G. Poschinger, F. Schmidt-Kaler, Transfer of optical orbital angular momentum to a bound electron. *Nat. Commun.* **7**, 12998 (2016).
9. H. He, M. E. J. Friese, N. R. Heckenberg, H. Rubinsztein-Dunlop, Direct observation of transfer of angular momentum to absorptive particles from a laser beam with a phase singularity. *Phys. Rev. Lett.* **75**, 826–829 (1995).
10. Z. Shen, Z. J. Hu, G. H. Yuan, C. J. Min, H. Fang, X.-C. Yuan, Visualizing orbital angular momentum of plasmonic vortices. *Opt. Lett.* **37**, 4627–4629 (2012).
11. W.-Y. Tsai, J.-S. Huang, C.-B. Huang, Selective trapping or rotation of isotropic dielectric microparticles by optical near field in a plasmonic archimedes spiral. *Nano Lett.* **14**, 547–552 (2014).
12. Y. Zhang, W. Shi, Z. Shen, Z. Man, C. Min, J. Shen, S. Zhu, H. P. Urbach, X. Yuan, A plasmonic spanner for metal particle manipulation. *Sci. Rep.* **5**, 15446 (2015).
13. J. Wang, J.-Y. Yang, I. M. Fazal, N. Ahmed, Y. Yan, H. Huang, Y. Ren, Y. Yue, S. Dolinar, M. Tur, A. E. Willner, Terabit free-space data transmission employing orbital angular momentum multiplexing. *Nat. Photonics* **6**, 488–496 (2012).
14. H. Ren, X. Li, Q. Zhang, M. Gu, On-chip noninterference angular momentum multiplexing of broadband light. *Science* **352**, 805–809 (2016).
15. Z. Yue, H. Ren, S. Wei, J. Lin, M. Gu, Angular-momentum nanometrology in an ultrathin plasmonic topological insulator film. *Nat. Commun.* **9**, 4413 (2018).
16. M. Erhard, R. Fickler, M. Krenn, A. Zeilinger, Twisted photons: New quantum perspectives in high dimensions. *Light Sci. Appl.* **7**, 17146 (2018).
17. E. Hasman, V. Kleiner, Spinoptics in plasmonics, in *Plasmonics: Theory and Applications* (Springer, 2013), pp. 463–499.
18. F. Cardano, L. Marrucci, Spin–orbit photonics. *Nat. Photonics* **9**, 776–778 (2015).
19. T. Ohno, S. Miyanishi, Study of surface plasmon chirality induced by Archimedes' spiral grooves. *Opt. Express* **14**, 6285–6290 (2006).
20. Y. Gorodetski, A. Niv, V. Kleiner, E. Hasman, Observation of the spin-based plasmonic effect in nanoscale structures. *Phys. Rev. Lett.* **101**, 043903 (2008).
21. Y. Gorodetski, N. Shitrit, I. Bretner, V. Kleiner, E. Hasman, Observation of optical spin symmetry breaking in nanoapertures. *Nano Lett.* **9**, 3016–3019 (2009).
22. S.-W. Cho, J. Park, S.-Y. Lee, H. Kim, B. Lee, Coupling of spin and angular momentum of light in plasmonic vortex. *Opt. Express* **20**, 10083–10094 (2012).
23. G. Spektor, D. Kilbane, A. K. Mahro, M. Hartelt, E. Prinz, M. Aeschlimann, M. Orenstein, Mixing the Light-spin with Plasmon-orbit by non-linear light matter interaction in gold. *Phys. Rev. X* **9**, 021031 (2019).
24. A. Kubo, N. Pontius, H. Petek, Femtosecond microscopy of surface plasmon polariton wave packet evolution at the silver/vacuum interface. *Nano Lett.* **7**, 470–475 (2007).
25. C. Lemke, C. Schneider, T. Leißner, D. Bayer, J. W. Radke, A. Fischer, P. Melchior, A. B. Evlyukhin, B. N. Chichkov, C. Reinhardt, M. Bauer, M. Aeschlimann, Spatiotemporal characterization of SPP pulse propagation in two-dimensional plasmonic focusing devices. *Nano Lett.* **13**, 1053–1058 (2013).
26. P. Kahl, S. Wall, C. Witt, C. Schneider, D. Bayer, A. Fischer, P. Melchior, M. H.-v. Hoegen, M. Aeschlimann, F.-J. Meyer zu Heringdorf, Normal-incidence photoemission electron microscopy (NI-PEEM) for imaging surface plasmon polaritons. *Plasmonics* **9**, 1401–1407 (2014).
27. G. Spektor, D. Kilbane, A. K. Mahro, B. Frank, S. Ristok, L. Gal, P. Kahl, D. Podbiel, S. Mathias, H. Giessen, F.-J. Meyer zu Heringdorf, M. Orenstein, M. Aeschlimann, Revealing

the subfemtosecond dynamics of orbital angular momentum in nanoplasmonic vortices. *Science* **355**, 1187–1191 (2017).
28. B. Frank, P. Kahl, D. Podbiel, G. Spektor, M. Orenstein, L. Fu, T. Weiss, M. Horn-von Hoegen, T. J. Davis, F.-J. Meyer zu Heringdorf, H. Giessen, Short-range surface plasmonics: Localized electron emission dynamics from a 60-nm spot on an atomically flat single-crystalline gold surface. *Sci. Adv.* **3**, e1700721 (2017).
29. D. Podbiel, P. Kahl, B. Frank, T. J. Davis, H. Giessen, M. H. Hoegen, F. J. Meyer zu Heringdorf, Spatiotemporal analysis of an efficient fresnel grating coupler for focusing surface plasmon polaritons. *ACS Photonics* **6**, 600–604 (2019).
30. Z. Liu, Y. Wang, J. Yao, H. Lee, W. Srituravanich, X. Zhang, Broad band two-dimensional manipulation of surface plasmons. *Nano Lett.* **9**, 462–466 (2009).
31. P. Dvořák, T. Neuman, L. Břínek, T. Šamořil, R. Kalousek, P. Dub, P. Varga, T. Šikola, Control and near-field detection of surface plasmon interference patterns. *Nano Lett.* **13**, 2558–2563 (2013).
32. G. Spektor, A. David, G. Bartal, M. Orenstein, A. Hayat, Spin-patterned plasmonics: Towards optical access to topological-insulator surface states. *Opt. Express* **23**, 32759–32765 (2015).
33. Y. Wang, Y. Xu, X. Feng, P. Zhao, F. Liu, K. Cui, W. Zhang, Y. Huang, Optical lattice induced by angular momentum and polygonal plasmonic mode. *Opt. Lett.* **41**, 1478–1481 (2016).
34. S. Tsesses, E. Ostrovsky, K. Cohen, B. Gjonaj, N. H. Lindner, G. Bartal, Optical skyrmion lattice in evanescent electromagnetic fields. *Science* **361**, 993–996 (2018).
35. S. Tsesses, K. Cohen, E. Ostrovsky, B. Gjonaj, G. Bartal, Spin–orbit interaction of light in plasmonic lattices. *Nano Lett.* **19**, 4010–4016 (2019).
36. T. J. Davis, D. Janoschka, P. Dreher, B. Frank, F.-J. M. zu Heringdorf, H. Giessen, Ultrafast vector imaging of plasmonic skyrmion dynamics with deep subwavelength resolution. *Science* **368**, eaba6415 (2020).
37. Y. Dai, Z. Zhou, A. Gosh, R. S. K. Mong, A. Kubo, C.-B. Huang, H. Petek, Plasmonic topological quasiparticle on the nanometre and femtosecond scales. *Nature* **588**, 616–619 (2020).
38. H. Ditlbacher, J. R. Krenn, G. Schider, A. Leitner, F. R. Aussenegg, Two-dimensional optics with surface plasmon polaritons. *Appl. Phys. Lett.* **81**, 1762–1764 (2002).
39. G. M. Lerman, A. Yanai, U. Levy, Demonstration of nanofocusing by the use of plasmonic lens illuminated with radially polarized light. *Nano Lett.* **9**, 2139–2143 (2009).
40. C. Schneider, *Mapping of Surface Plasmon Polariton Fields by Time-Resolved Photoemission Electron Microscopy: Experiments, Simulations, Applications* (Verlag Dr. Hut, 2013).
41. J. Dong, J. Wang, F. Ma, Y. Cheng, H. Zhang, Z. Zhang, Recent progresses in integrated nanoplasmonic devices based on propagating surface plasmon polaritons. *Plasmonics* **10**, 1841–1852 (2015).
42. G. Spektor, A. David, B. Gjonaj, L. Gal, G. Bartal, M. Orenstein, Linearly dichroic plasmonic lens and hetero-chiral structures. *Opt. Express* **24**, 2436–2442 (2016).
43. J. Lin, J. P. B. Mueller, Q. Wang, G. Yuan, N. Antoniou, X.-C. Yuan, F. Capasso, Polarization-controlled tunable directional coupling of surface plasmon polaritons. *Science* **340**, 331–334 (2013).
44. H. Kim, J. Park, S.-W. Cho, S.-Y. Lee, M. Kang, B. Lee, Synthesis and dynamic switching of surface plasmon vortices with plasmonic vortex lens. *Nano Lett.* **10**, 529–536 (2010).
45. E. Ostrovsky, K. Cohen, S. Tsesses, B. Gjonaj, G. Bartal, Nanoscale control over optical singularities. *Optica* **5**, 283–288 (2018).
46. N. Shitrit, I. Bretner, Y. Gorodetski, V. Kleiner, E. Hasman, Optical spin hall effects in plasmonic chains. *Nano Lett.* **11**, 2038–2042 (2011).
47. G. Spektor, A. David, B. Gjonaj, G. Bartal, M. Orenstein, Metafocusing by a metaspiral plasmonic lens. *Nano Lett.* **15**, 5739–5743 (2015).
48. C.-F. Chen, C.-T. Ku, Y.-H. Tai, P.-K. Wei, H.-N. Lin, C.-B. Huang, Creating optical near-field orbital angular momentum in a gold metasurface. *Nano Lett.* **15**, 2746–2750 (2015).
49. Q. Tan, Q. Guo, H. Liu, X. Huang, S. Zhang, Controlling the plasmonic orbital angular momentum by combining the geometric and dynamic phases. *Nanoscale* **9**, 4944–4949 (2017).
50. Q. Tan, Z. Xu, D. H. Zhang, T. Yu, S. Zhang, Y. Luo, Polarization-controlled plasmonic structured illumination. *Nano Lett.* **20**, 2602–2608 (2020).
51. Y. Yang, G. Thirunavukkarasu, M. Babiker, J. Yuan, Orbital-angular-momentum mode selection by rotationally symmetric superposition of chiral states with application to electron vortex beams. *Phys. Rev. Lett.* **119**, 094802 (2017).
52. E. Prinz, G. Spektor, M. Hartelt, A.-K. Mahro, M. Aeschlimann, M. Orenstein, Functional meta lenses for compound plasmonic vortex field generation and control. *Nano Lett.* **21**, 3941–3946 (2021).
53. S. J. P. Kress, F. V. Antolinez, P. Richner, S. V. Jayanti, D. K. Kim, F. Prins, A. Riedinger, M. P. C. Fischer, S. Meyer, K. M. McPeak, D. Poulikakos, D. J. Norris, Wedge waveguides and resonators for quantum plasmonics. *Nano Lett.* **15**, 6267–6275 (2015).
54. Z. Fang, Q. Peng, W. Song, F. Hao, J. Wang, P. Nordlander, X. Zhu, Plasmonic focusing in symmetry broken nanocorrals. *Nano Lett.* **11**, 893–897 (2011).
55. E. A. Weiss, G. K. Kaufman, J. K. Kriebel, Z. Li, R. Schalek, G. M. Whitesides, Si/SiO_2-templated formation of ultraflat metal surfaces on glass, polymer, and solder supports: Their use as substrates for self-assembled monolayers. *Langmuir* **23**, 9686–9694 (2007).
56. D. Yoo, T. W. Johnson, S. Cherukulappurath, D. J. Norris, S.-H. Oh, Template-stripped tunable plasmonic devices on stretchable and rollable substrates. *ACS Nano* **9**, 10647–10654 (2015).
57. N. Vogel, J. Zieleniecki, I. Köper, As flat as it gets: Ultrasmooth surfaces from template-stripping procedures. *Nanoscale* **4**, 3820–3832 (2012).
58. M. U. González, J.-C. Weeber, A.-L. Baudrion, A. Dereux, A. L. Stepanov, J. R. Krenn, E. Devaux, T. W. Ebbesen, Design, near-field characterization, and modeling of 45° surface-plasmon Bragg mirrors. *Phys. Rev. B* **73**, 155416 (2006).
59. L. D. Landau, E. M. Lifshitz, L. P. Pitaevskii, Electrodynamics of Continuous Media (Pergamon Press Ltd., 1984).
60. M. U. Wehner, M. H. Ulm, M. Wegener, Scanning interferometer stabilized by use of Pancharatnam's phase. *Opt. Lett.* **22**, 1455–1457 (1997).

Acknowledgments: We acknowledge the Micro-Nano Fabrication Unit (MNFU) Technion for support with sample fabrication. We acknowledge G. Ankonina for the sputtering of gold, J. Schnider for help with thermal oxide growing, L. Gal for e-beam gold deposition, and L. Popilevsky for assistance with focused ion beam milling. **Funding:** G.S. and M.O. acknowledge support from the Israeli Centers of Research Excellence "Circle of Light." G.S. would like to acknowledge the support from the Clore Israel Foundation and the Schmidt Science Fellowship. E.P. acknowledges support from the Max Planck Graduate Center with the Johannes Gutenberg University Mainz and the TU Kaiserslautern through a PhD fellowship.
Author contributions: G.S., M.O., and M.A. conceived the idea and experiment. A.-K.M., M.H., and E.P. performed the experiment. G.S. performed the theory, modeling, sample design, and fabrication. Data analysis and interpretation performed by G.S., M.H., and E P. All authors assisted in understanding and interpreting the data. This paper is written by G.S., E P., and M.H. with contributions from all authors. **Competing interests:** The authors declare that they have no competing interests. **Data and materials availability:** All data needed to evaluate the conclusions in the paper are present in the paper and/or the Supplementary Materials. In addition, raw data from which the material in this work was evaluated are available at https://doi.org/10.5281/zenodo.4773044. Additional data related to this paper may be requested from the authors.

Submitted 13 January 2021
Accepted 23 June 2021
Published 11 August 2021
10.1126/sciadv.abg5571

Citation: G. Spektor, E. Prinz, M. Hartelt, A.-K. Mahro, M. Aeschlimann, M. Orenstein, Orbital angular momentum multiplication in plasmonic vortex cavities. *Sci. Adv.* **7**, eabg5571 (2021).